

# Giant Variations of Cooper-Pair Size in Nanoscale Superconductors

A. A. Shanenko,<sup>1</sup> M. D. Croitoru,<sup>1,2</sup> A. Vagov,<sup>2</sup> and F. M. Peeters<sup>1</sup>

<sup>1</sup>*Departement Fysica, Universiteit Antwerpen, Groenenborgerlaan 171, B-2020 Antwerpen, Belgium*

<sup>2</sup>*University of Bayreuth, Institute of Theoretical Physics, D-95440 Bayreuth, Germany*

(Dated: October 26, 2018)

The Cooper-pair size (i.e., the BCS coherence length) in low-dimensional superconductors is dramatically modified by quantum-size effects. In particular, for nanowires made of conventional superconducting materials, we show that the coherence length exhibits size-dependent drops by two-three orders of magnitude and reaches values found in high- $T_c$  superconductors. This phenomenon is surprisingly similar to the well-known BCS-BEC crossover but with one important exception: it is driven by the transverse quantization of the electron spectrum rather than by the strength of the fermion-fermion interaction. Similar results can be expected for other systems with the same structure of the single-particle spectrum, e.g. for superfluid Fermi gases confined in a quantum-wire or quantum-well geometry.

PACS numbers: 74.78.-w, 74.78.Na

Superconductors of ultra-small dimensions possess unusual properties not found in bulk materials. One of them is the *quantum-size oscillations*, first discussed by Blatt and Thompson [1]. In quasi-1D and -2D superconducting systems (nanowires and nanofilms) quantization of the transverse electron motion results in single-electron subbands, i.e., in multiple quantum channels for the superconducting condensate. The proximity of the lower edge of a single-electron subband to the Fermi surface leads to a size-dependent enhancement of superconducting properties, i.e., the *superconducting resonance*. In particular, such resonances are expected to strongly influence the critical temperature and critical magnetic field (see, e.g., Refs. 1, 2, 3, 4). Furthermore, they can lead to a remarkable cascade structure of the superconductor-to-normal transition [4] and can result in the appearance of a new type of Andreev states induced by quantum confinement [5].

For conventional materials, e.g., Al, Sn or Pb, the superconducting gap is about 0.1 – 1.0 meV [6] and, so, the inter-subband energy spacing  $\frac{\hbar^2}{2m_e} \frac{\pi^2}{d^2}$  (with  $d$  the confining dimension) becomes of the same order or larger for  $d \lesssim 20 - 40$  nm, where quantum-size oscillations of the superconducting properties are expected to be significant. Several recent experimental results on superconducting Pb nanofilms [7, 8] and superconducting aluminum/tin nanowires [9] have been attributed to these quantum-size effects (see Refs. 7, 8 and 3, respectively).

In the present Letter we report an unexpected phenomenon which is due to quantum-size effects, i.e., giant variations of the Cooper-pair size (i.e., the BCS coherence length  $\xi_0$ ) in low-dimensional superconductors. In all previous theoretical studies of superconducting nanowires and nanofilms, e.g., modeling phase-slip effects in nanowires (see, e.g., Ref. 9), one assumes that  $\xi_0$  is specified by the same expressions as in bulk. Contrary to this common expectation, our numerical investigations of the Bogoliubov-de Gennes equations [6] for

a clean superconducting quantum wire made of conventional materials reveal that, depending on the wire width, the longitudinal Cooper-pair size varies several orders of magnitude, from values of a few micrometers, typical for conventional bulk superconductors, to a few nanometers, that is usually found in high- $T_c$  materials [10]. This phenomenon turns out to be very similar to the BCS-BEC crossover in superfluid Fermi gases [11]. However, in the present case a giant drop in the Cooper-pair size is induced by quantum-size effects rather than by a change in the strength of the fermion-fermion interaction. Our results are not only relevant for superconducting quantum wires but are also applicable to other systems with a similar single-particle spectrum, e.g., to ultrathin superconducting metallic nanofilms and ultracold Fermi gases confined in a quantum-wire or quantum-well geometry.

*Model and formalism.* – We consider a superconducting nanocylinder in the clean limit. For our numerical calculations we take the material parameters of aluminum, the same as in Refs. [3, 4, 5]:  $\hbar\omega_D = 32.31$  meV;  $gN(0) = 0.18$  (with  $N(0)$  the bulk DOS); and  $E_F = 0.9$  eV is the effective Fermi level in the parabolic band approximation (for more details, see Ref. 3). Two values for the wire diameter are investigated below:  $d = 4.22$  nm, for which the wire is in the resonance conditions, i.e., the bottom of one of the single-electron subbands is close to the Fermi level; and  $d = 4.35$  nm, when the wire is not influenced by a superconducting resonance. We note that our conclusions are not sensible to a particular choice of the parameters as long as  $d \lesssim 10 - 15$  nm; in the wires of larger diameters quantum-size effects play less serious role.

Internal structure of Cooper pairs is described by  $\Psi(\mathbf{x}_1, \mathbf{x}_2)$  (the Cooper-pair wave function) which is related to the anomalous Green's function as

$$\Psi(\mathbf{x}_1, \mathbf{x}_2) = i \lim_{t_1 \rightarrow t_2 + 0} \mathcal{F}(\mathbf{x}_1 t_1, \mathbf{x}_2 t_2), \quad (1)$$

where  $\mathcal{F}(\mathbf{x}_1 t_1, \mathbf{x}_2 t_2) = \frac{1}{i} \langle \mathcal{T} \psi_\uparrow(\mathbf{x}_1 t_1) \psi_\downarrow(\mathbf{x}_2 t_2) \rangle$  (for the

spin-singlet pairing). In what follows we use cylindrical coordinates  $\mathbf{x} = (\rho, \varphi, z)$ . The diagonal part of Eq. (2), i.e., at  $\mathbf{x}_1 = \mathbf{x}_2 = \mathbf{x}$ , is directly related to the superconducting order parameter  $\Delta(\mathbf{x}) = g\Psi(\mathbf{x}, \mathbf{x})$ , where  $g > 0$  is the Gor'kov coupling constant. Rotational and translational (along the wire) symmetries of the system are reflected in  $\Psi(\mathbf{x}_1, \mathbf{x}_2)$  which depends on  $\phi = \varphi_1 - \varphi_2$  and  $z = z_1 - z_2$ . In turn, the order parameter is a function of  $\rho$  only. Here, we are interested in the structure of a Cooper pair along the wire and, therefore, consider the quantity

$$\Psi(\rho, z) = \Psi(\rho, \varphi, z_1 + z; \rho, \varphi, z_1). \quad (2)$$

The anomalous Green's function can be expressed in terms of the eigenstates of the BdG equations (see, e.g., [6]) which, following the system symmetry, are specified by the radial quantum number  $j$ , azimuthal quantum number  $m$  and wavevector  $k$  of the quasi-free particle motion along the wire. This defines 1D subbands labeled as  $(j, m)$ . For  $T = 0$  the wave function in Eq. (2) can be written as a sum over such subbands as

$$\Psi(\rho, z) = \sum_{jm} \Psi_{jm}(\rho, z), \quad (3)$$

with the subband contribution given by

$$\Psi_{jm}(\rho, z) = \frac{1}{(2\pi)^2} \int dk u_{jmk}(\rho) v_{jmk}^*(\rho) e^{ikz}. \quad (4)$$

Here  $u_{jmk}(\rho)$  and  $v_{jmk}(\rho)$  obey the BdG equations written as

$$E_{jmk} \begin{pmatrix} u_{jmk} \\ v_{jmk} \end{pmatrix} = \begin{pmatrix} \hat{H}_{mk} & \Delta(\rho) \\ \Delta^*(\rho) & -\hat{H}_{mk}^* \end{pmatrix} \begin{pmatrix} u_{jmk} \\ v_{jmk} \end{pmatrix}, \quad (5)$$

with  $E_{jmk}$  the quasiparticle energy and

$$\hat{H}_{mk} = -\frac{\hbar^2}{2m_e} \left[ \frac{1}{\rho} \frac{\partial}{\partial \rho} \rho \frac{\partial}{\partial \rho} - \frac{m^2}{\rho^2} - k^2 \right] - E_F,$$

where  $m_e$  is the electron band mass taken equal to the free-electron mass. Solutions of Eq. (5) are set to be zero at the wire boundary (quantum-confinement boundary conditions).

*Resonant subbands, qualitative picture.* – The integral over  $k$  in Eq. (4) is restricted to the Debye window, i.e.,  $|\xi_{jmk}| < \hbar\omega_D$ , where  $\xi_{jmk}$  is the subband single-particle dispersion  $\xi_{jmk} = \hbar^2 k^2 / 2m_e - \mu_{jm}$  with  $\mu_{jm} = E_F - \varepsilon_{jm}$  the subband chemical potential and  $\varepsilon_{jm}$  the subband lower edge (bottom) energy. Figure 1(a) shows a sketch of the single-particle energies for the subbands with  $j = 0$  and  $m = 0, \pm 1, \pm 2$ . The dotted horizontal lines in Fig. 1(a) highlight the Debye window that determines the upper  $k_{jm}^+$  and lower  $k_{jm}^-$  limits for  $k$  in the integral in Eq. (4).

The bottoms of all single-electron subbands shift in energy with changing diameter. A quantum-size superconducting resonance occurs when the bottom of a subband

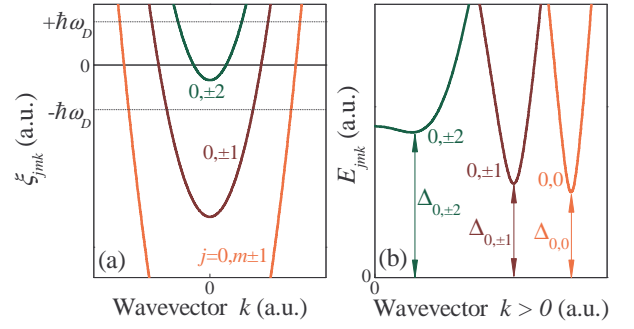


FIG. 1: (Color online) (a) Single-electron energies  $\xi_{jmk}$  (measured from the Fermi level  $E_F$ ) versus the wavevector for the longitudinal motion  $k$  in subbands  $(j, m) = (0, 0), (0, \pm 1)$  and  $(j, \pm 2)$ . Horizontal dotted lines denote the Debye window. (b) Quasiparticle energies  $E_{jmk}$  as function of  $k$  for the same subbands.

comes into the Debye window, i.e., when  $|\mu_{jm}| < \hbar\omega_D$  and  $k_{jm}^- = 0$ . In Fig. 1(a) subbands  $(0, \pm 2)$  satisfy this condition. Below they are referred to as resonant subbands. Any subband generates a quantum channel for the formation of the superconducting condensate. In a simplified picture one can utilize Anderson's approximate solution of the BdG equations (see, e.g., Ref. [4]), which assumes that the spatial dependence of both  $u_{jmk}(\rho)$  and  $v_{jmk}(\rho)$  is given by the radial single-electron wave function  $\vartheta_{jm}(\rho)$  (proportional to the Bessel function of the first kind). This leads to  $E_{jmk} = (\xi_{jmk}^2 + \Delta_{jm}^2)^{1/2}$ , with  $\Delta_{jm}$  the subband energy gap as schematically shown in Fig. 1(b).

Within Anderson's approximation, Eq. (4) reduces to

$$\Psi_{jm}(\rho, z) = \frac{\vartheta_{jm}(\rho)^2}{(2\pi)^2} \int_{k_{jm}^-}^{k_{jm}^+} dk \frac{\Delta_{jm} \cos(kz)}{\sqrt{\xi_{jmk}^2 + \Delta_{jm}^2}}. \quad (6)$$

In most cases the integration limits in Eq. (6) can be extended to infinity. This yields an exponentially decaying function of  $z$ , and its characteristic decay length defines the subband (channel) BCS coherence length

$$\xi_0^{(jm)} = \frac{\hbar}{\sqrt{m_e}} \left[ \sqrt{\mu_{jm}^2 + \Delta_{jm}^2} - \mu_{jm} \right]^{-1/2}. \quad (7)$$

As seen from Eq. (7),  $\xi_0^{(jm)}$  decreases when  $\mu_{jm}$  goes from positive to negative values. In the limit  $\mu_{jm}/\Delta_{jm} \gg 1$  we have the conventional result for the BCS coherence length, which reads as  $\xi_0^{(jm)} \approx \hbar v_{jm}/\Delta_{jm}$ , with  $v_{jm} = \sqrt{2\mu_{jm}/m_e}$  the subband Fermi wavevector. At resonance, i.e., for  $\mu_{jm} \rightarrow 0$ , we find from Eq. (7) a very different expression  $\xi_0^{(jm)} \approx \hbar/(m_e \Delta_{jm})^{1/2}$ . Finally, when  $\mu_{jm} < 0$  and  $|\mu_{jm}| \gg \Delta_{jm}$ , we obtain  $\xi_0^{(jm)} \approx \hbar/(2m_e |\mu_{jm}|)^{1/2}$ , which decreases with increasing  $|\mu_{jm}|$ . Thus, we have a drop in the BCS coherence length of the resonant subband(s) and, at the same

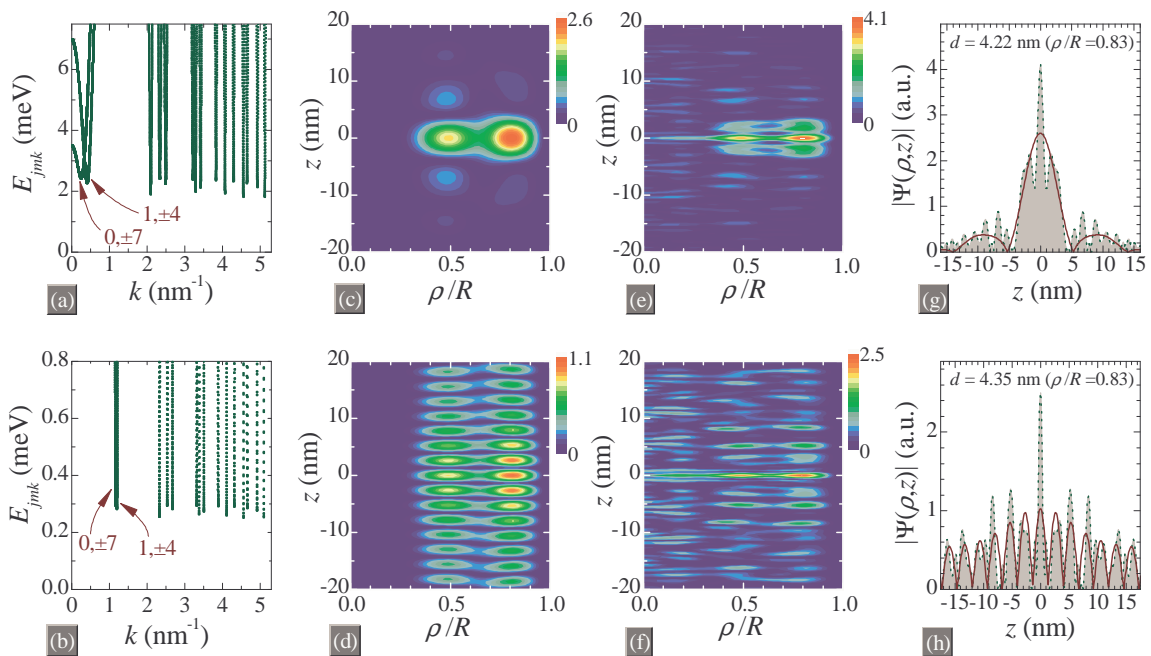


FIG. 2: (Color online) The resonant wire,  $d = 4.22$  nm: (a) the quasiparticle-energy dispersion  $E_{jmk}$ , the resonant subbands are  $(j, m) = (0, \pm 7)$  and  $(1, \pm 4)$ ; (c) the contour plot of  $|\Psi(\rho, z)|$  (arbitrary units) when accounting only for subbands  $(0, \pm 7)$  and  $(1, \pm 4)$ ; (e) the same but for the total Cooper-pair wave function; (g) the longitudinal profile of  $|\Psi(\rho, z)|$  at  $\rho/R = 0.83$  with all relevant quantum channels included (dotted curve) and when only contributions of  $(0, \pm 7)$  and  $(1, \pm 4)$  are taken (solid red curve). Panels (b), (d), (e), (f) display the same but for the non-resonant wire at  $d = 4.35$  nm.

time, such a subband(s) provides a major contribution to Eq. (3) due to a significantly enhanced DOS in the Debye window.

It is surprising that for  $\mu_{jm} < 0$ , Eq. (7) is reduced to the expression for the fermion-pair size at the BEC side of the BCS-BEC crossover in superfluid Fermi gases (see discussion after Eq. (140) in Ref. 11). However, in our case  $\mu_{jm}$  becomes negative due to quantum-size effects instead of a change in the strength of the pair interaction (for numerical details, see Fig. 3 and discussion below).

*Numerical solution.* – A numerical self-consistent solution of the BdG equations (5) give the results shown in Figs. 2 and 3. In Fig. 2(a) the quasiparticle energies  $E_{jmk}$  are given versus  $k$  for  $d = 4.22$  nm. Here the bottoms of the two single-electron subbands with  $(j, m) = (0, \pm 7)$  and  $(1, \pm 4)$  are in the Debye window and, so,  $v_{0, \pm 7}$  and  $v_{1, \pm 4}$  (recall that  $v_{jm} = \sqrt{2\mu_{jm}/m_e}$ ) are extremely small. The quasiparticle spectrum for the non-resonant wire with  $d = 4.35$  nm is shown in Fig. 2(b). The corresponding single-electron spectrum has no resonant subbands and  $v_{0, \pm 7}$  and  $v_{1, \pm 4}$  are larger by an order of magnitude as compared to panel (a). Numerical results for the resonant case exhibit a significant increase of  $\Delta_{0, \pm 7}$  and  $\Delta_{1, \pm 4}$  and, in turn, lead to enhanced superconducting gaps in the other quantum channels. When the resonance decays (i.e., due to a change in  $d$ ), all  $\Delta_{jm}$  are reduced and approach the bulk value  $\Delta_{\text{bulk}} = 0.25$  meV.

The contour plots in Figs. 2(c) and (d), for the res-

onant and non-resonant wires, respectively, display the absolute value of  $\Psi(\rho, z)$ , as calculated from Eq. (3) but with the summation restricted to subbands  $(0, \pm 7)$  and  $(1, \pm 4)$ . Panels (e) [for  $d = 4.22$  nm] and (f) [for  $d = 4.35$  nm] show the total quantity  $|\Psi(\rho, z)|$ , where we summed over all relevant subbands. For the resonant case, illustrated by panels (c) and (e), the longitudinal distribution of electrons is well localized, whereas an oscillating and weakly decaying dependence appear in panels (d) and (f). This is also clearly seen from panels (g) and (h) representing the longitudinal profile of  $|\Psi(\rho, z)|$  at  $\rho/R = 0.83$  [i.e., the maximum point of  $\Psi(\rho, z = 0)$ ] for the resonant and non-resonant wires, respectively. Here the dotted curve gives the total contribution of all subbands whereas the solid line corresponds to a contribution from only  $(j, m) = (0, \pm 7)$  and  $(1, \pm 4)$ . Thus, the resonant subbands control  $\Psi(\rho, z)$  for the resonant wire, and the corresponding longitudinal distribution of electrons in a Cooper pair is strongly localized. At  $d = 4.35$  nm single-electron subbands  $(j, m) = (0, \pm 7)$  and  $(1, \pm 4)$  are shifted down as compared to their positions at  $d = 4.22$  nm. As a result, the resonance disappears and the relative contribution of the states with  $(j, m) = (0, \pm 7)$  and  $(1, \pm 4)$  to the superconducting order parameter  $\Delta(\rho) = \Psi(\rho, z = 0)$  drops to 40%, see panel (h). Nevertheless, the longitudinal decay of the correlation function  $\Psi(\rho, z)$  is still mainly determined by these states.

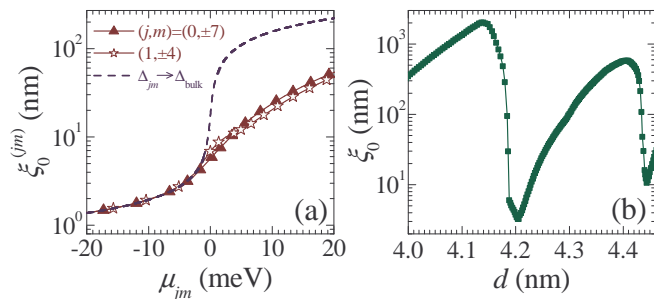


FIG. 3: (Color online) BCS-BEC crossover induced by quantum-size effects: (a) the subband longitudinal BCS coherence length  $\xi_0^{(jm)}$  versus  $\mu_{jm}$  as numerically calculated from the BdG equations for  $(j, m) = (0, \pm 7)$  (triangles) and  $(1, \pm 4)$  (stars), the dashed curve represents Eq. (7) with  $\Delta_{jm}$  replaced by  $\Delta_{\text{bulk}}$ ; (b) the total longitudinal BCS coherence length  $\xi_0$  versus the nanowire diameter.

The longitudinal BCS coherence length is defined as the decay length of  $\Psi(\rho, z)$  in the  $z$  direction and can be calculated through a numerical fit. For both the partial and total wave functions, such a fitting gives similar values:  $\sim 1 \mu\text{m}$  for the non-resonant wire and  $\approx 5 \text{ nm}$  for the resonant case. The latter value is almost three orders of magnitude less than the BCS coherence length in bulk aluminum ( $\approx 1.6 \mu\text{m}$ ) and is comparable to the one in high- $T_c$  superconductors [10]. Further insight can be obtained from Figs. 3(a) and (b). Panel (a) demonstrates numerical results for  $\xi_0^{(jm)}$  as function of  $\mu_{jm}$  for  $(j, m) = (0, \pm 7)$  (triangles) and  $(1, \pm 4)$  (stars). Notice that these data are in good agreement with the analytical formula of Eq. (7). When substituting  $\Delta_{\text{bulk}}$  for  $\Delta_{jm}$  in Eq. (7), we obtain the dashed curve approaching our numerical results for  $\mu_{jm} < 0$ . In this case  $\xi_0^{(jm)} \approx \hbar/(2m_e|\mu_{jm}|)^{1/2}$  is not sensitive any more to  $\Delta_{jm}$ . Finally, Fig. 3(b) illustrates how the total longitudinal BCS coherence length  $\xi_0$  depends on  $d$ . Its value is minimal at  $d = 4.22 \text{ nm}$ , and the difference between the maximum and minimum is roughly two-three orders of magnitude. As seen from Fig 3(b), the next superconducting resonance comes into play at  $d = 4.44 \text{ nm}$ . Notice that when increasing  $d$ , quantum-size oscillations of  $\xi_0$  are weakened and washed out for  $d \gtrsim 30 - 40 \text{ nm}$ .

*Conclusions.* – We have demonstrated that the longitudinal Cooper-pair size in a superconducting metallic nanowire undergoes size-dependent giant drops driven by the transverse quantization of the electron spectrum. As

a result, the BCS coherence length of a quantum wire made of conventional materials acquires values typical for high- $T_c$  superconductors. A striking feature of this phenomenon is that it is very similar to the BCS-BEC crossover found in superfluid Fermi gases. However, there is a very important difference: a giant drop of the longitudinal Cooper-pair size in our quantum superconducting wire is a result of the transverse quantization of the electron motion while the BCS-BEC crossover in superfluid Fermi gases is realized by changing the inter-particle interaction strength. Notice that the same qualitative behavior can be found for different values of the material parameters and a sharp Debye window is not essential. Therefore, such a phenomenon is a generic feature that will be present in other low-dimensional systems, where the condensate is formed via multiple quantum-size channels, e.g., in superconducting nanofilms and ultracold Fermi gases confined in a quantum-wire or quantum-well geometry [11].

This work was supported by the Flemish Science Foundation (FWO-VI), the Belgian Science Policy (IAP) and the ESF-network: INSTANS.

- 
- [1] J. M. Blatt and C. J. Thompson, Phys. Rev. Lett. **10**, 332 (1963).
  - [2] M. Strongin, R. S. Thompson, O. F. Kammerer, and J. E. Crow, Phys. Rev. B **1**, 1078 (1970); B. Chen, Z. Zhu, and X. C. Xie, Phys. Rev. B **74**, 132504 (2006).
  - [3] A. A. Shanenko, M. D. Croitoru, M. Zgirski, F. M. Peeters, and K. Arutyunov, Phys. Rev. B **74**, 052502 (2006); A. A. Shanenko, M. D. Croitoru, and F. M. Peeters, Phys. Rev. B **75**, 014519 (2007).
  - [4] A. A. Shanenko, M. D. Croitoru, and F. M. Peeters, Phys. Rev. B **78**, 054505 (2008).
  - [5] A. A. Shanenko, M. D. Croitoru, R. G. Mints, and F. M. Peeters, Phys. Rev. Lett. **99**, 067007 (2007).
  - [6] P. G. de Gennes, 1966. *Superconductivity of Metals and Alloys* (W. A. Benjamin, New York, 1966).
  - [7] Y. Guo et al., Science **306**, 1915 (2004).
  - [8] D. Eom, S. Qin, M.-Y. Chou, and C. K. Shih, Phys. Rev. Lett. **96**, 027005 (2006).
  - [9] K. Yu. Arutyunov, D.S. Golubev, and A.D. Zaikin, Phys. Rep. **464**, 1 (2008).
  - [10] G. Deutscher, *New Superconductors: From Granular to High  $T_c$*  (World Scientific, Singapore, 2006).
  - [11] I. Bloch, J. Dalibard, and W. Zwerger, Rev. Mod. Phys. **80**, 885 (2008).